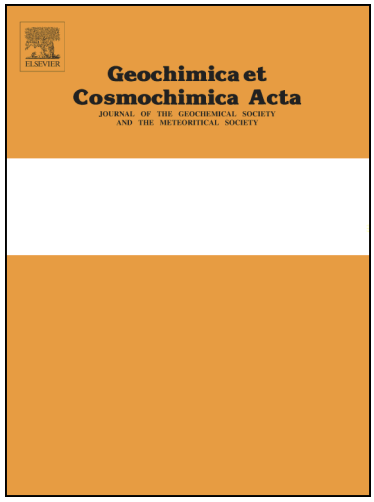

In situ study of boron partitioning between calcite and fluid at different crystal growth rates

Rinat I. Gabitov, Claire Rollion-Bard, Aradhna Tripati, Aleksey Sadekov

PII: S0016-7037(14)00248-8
DOI: http://dx.doi.org/10.1016/j.gca.2014.04.014
Reference: GCA 8766

To appear in: *Geochimica et Cosmochimica Acta*

Received Date: 30 October 2012
Accepted Date: 4 April 2014

Please cite this article as: Gabitov, R.I., Rollion-Bard, C., Tripati, A., Sadekov, A., *In situ* study of boron partitioning between calcite and fluid at different crystal growth rates, *Geochimica et Cosmochimica Acta* (2014), doi: http://dx.doi.org/10.1016/j.gca.2014.04.014

In situ study of boron partitioning between calcite and fluid at different crystal growth rates

Rinat I. Gabitov[1*], Claire Rollion-Bard[2,ϕ], Aradhna Tripati[3], and Aleksey Sadekov[4]
[1] Mississippi State University, Mississippi State, MS, 39762, USA (*correspondence: rinat.gabitov@gmail.com);
[2] Centre de Recherches Pétrographiques et Géochimiques, CRPG-CNRS, Université de Lorraine, UMR 7358, BP 20, F-54501 Vandoeuvre-Les-Nancy Cedex, France;
[3] University of California, Los Angeles, CA, 90095, USA;
[4] University of Cambridge, Cambridge, CB23EQ, UK
[ϕ]present address: Institut de Physique du Globe de Paris (IPGP), Université Paris Diderot, UMR CNRS 7154, 1 rue Jussieu, F-75238 Paris Cedex 05, France

Abstract

The boron isotopic and chemical content of carbonates (expressed as $\delta^{11}B$ and B/Ca ratios) have been proposed as proxies for seawater carbonate system parameters. Thermodynamic and kinetic effects on $\delta^{11}B$ and B partitioning are not yet fully constrained, underscoring the importance of exploring possible effects of growth rate on boron incorporation in synthetic calcium carbonate minerals, which is the focus of this study. Secondary Ion Mass Spectrometry (SIMS) measurements of B/Ca and $\delta^{11}B$ were performed on single crystals of calcite synthesized by diffusion of CO_2 under controlled conditions from a solution of NH_4Cl-$CaCl_2$ doped with boron. Growth rates of calcite (V, nm/s) within crystals grown isothermally at 24.6°C were monitored by sequentially spiking calcite-precipitating fluids with rare earth element (REE) dopants. The REE were analyzed with SIMS at spots that match those locations where B/Ca and $\delta^{11}B$ ratios were measured. Values for the boron Nernst partition coefficient, defined as $D_B=B_{(calcite)}/B_{(fluid)}$, increase from 0.5 ($pH_{NBS}$=8.15) to 0.9 (pH=8.00) with values of V increasing from 0.04

to 0.13 nm/s. For $\delta^{11}B$ behavior, it was not possible to draw conclusive results due to the analytical error (2.2 ‰; 2σ). pH effects on D_B during calcite precipitation, associated with an increase in pH from 8.00 to 8.15, appear to be masked by the competing effects of changing V. We conclude that over the range of growth rates and other conditions investigated in this study, growth rate effects on B partitioning need to be accounted for when using B/Ca ratios in biogenic calcite as a proxy for seawater carbonate system parameters.

Keywords:
Calcite
Boron
Isotopes
Fractionation factor
Partition coefficient
Growth rate
SIMS
Equilibrium

1. INTRODUCTION

Dissolved inorganic boron in fluids is present mainly as the two chemical species $B(OH)_3$ and $B(OH)_4^-$, with the fraction of each species present dependent on solution pH at equilibrium (Hershey et al., 1986; Hemming and Hanson, 1992). There is an isotopic fractionation between these two species of about 27.2 ‰ (Klochko et al., 2006), with $B(OH)_3$ being enriched in ^{11}B. It is generally assumed that only $B(OH)_4^-$ is incorporated into calcite (Hemming et al., 1995). Thus the partition coefficient of boron, as defined in Hemming and Hanson (1992), has been proposed as a proxy for solution $[B(OH)_4^-]/[HCO_3^-]$ ratios (Yu and Elderfield, 2007; Yu et al., 2007a, b; Tripati et al., 2009, 2011; Allen et al., 2012), as well as the $[CO_3^{2-}]$ of seawater (Yu and Elderfield, 2007; Rae et al., 2011). Furthermore, the boron isotopic composition of carbonates has been used as a

proxy for the pH of solution from which carbonate minerals precipitate (e.g. Spivack et al., 1987; Sanyal et al., 1997; Palmer et al., 1998; Hobbs and Reardon, 1999; Pearson and Palmer, 2000, amongst many other references). As the boron isotopic composition and boron content of calcium carbonate minerals (expressed as $\delta^{11}B$ and B/Ca) depend on seawater carbonate system parameters, they have been used as proxies for ancient seawater pH, $[B(OH)_4^-]/[HCO_3^-]$, and $[CO_3^{2-}]$.

The sensitivity of carbonate $\delta^{11}B$ and B to seawater pH and dissolved inorganic carbon (DIC) leads to a relationship between these seawater carbonate system proxies and partial pressure of CO_2 in the atmosphere (pCO_2). Atmospheric pCO_2 is a key parameter in studies of Earth's climate in the past, and reconstructed ancient values are used to quantify the link between past climate changes and atmospheric paleo-pCO_2 fluctuations and better constrain models that are used for studying future climate variations. An additional importance of these seawater carbonate system proxies stems from the continuing acidification of the ocean through emissions of anthropogenic CO_2 into the atmosphere and the impact of this acidification on calcifying species (Orr et al., 2005; Gattuso and Hansson, 2011).

However, the B content and $\delta^{11}B$ composition of biogenic carbonates exhibit some evidence for taxon-specific partitioning, also termed "vital" effects (e.g. Zeebe et al, 2003; Sanyal et al., 1996, 2001; Pagani et al. 2005; Yu et al., 2007a,b; Tripati et al., 2011). These vital effects could be due in part to the increase of the pH of the solution before carbonate precipitation as has been hypothesized and observed in foraminifera and in corals (e.g. McConnaughey, 1989; Adkins et al, 2003; Hönisch et al, 2004; Rollion-Bard et al., 2003, 2011; Blamart et al., 2007; de Nooijer et al., 2009; Allison et al., 2010;

Rollion-Bard and Erez, 2010; Ries, 2011). Another factor that may be important is potential kinetic effects on $\delta^{11}B$ and B partitioning into carbonates. These effects are not yet well constrained, underscoring the importance of exploring effect of growth rate (V, nm/s) on $\delta^{11}B$ and B fractionation in synthetic calcium carbonate minerals, which is the focus of this study.

It has been established that growth rate has a significant effect on the incorporation of a range of divalent cations into calcite (Lorens 1981; Tesoriero and Pankow 1996; Gabitov and Watson 2006; Tang et al. 2008a; Gabitov et al. 2014). Previous experimental data on B partitioning between calcite and fluid have yielded $D_B=B_{crystal}/B_{fluid}=3.1\pm0.06$ (bulk isotope dilution analytical method; B_{fluid}=44 ppm, Ca_{fluid}=5370 ppm or 0.134 mol/l) at T=20°C (Hemming et al. 1995). In contrast, the *in situ* SIMS data of Hemming et al. (1998) indicated D_B ranging from 0.11 to 1.86 ±20% between different vicinal faces on a calcite $\{10\bar{1}4\}$ face as measured on two crystals grown in the same experiment by Hemming et al. (1995).

Here we investigate the potential influence of growth rate on the B content and boron isotopic composition of calcite crystal and discuss the implications for using B/Ca ratios in naturally-occurring carbonates as carbonate system proxies. Briefly, we determined growth rates by injecting rare-earth element (REE) spikes into the growth medium at discrete intervals during crystallization (see Gabitov et al. (2012) for more details), and then measured the amount of crystal growth between the spikes to calculate growth rates. We used *in situ* SIMS analyses to determine B and $\delta^{11}B$ in each REE-marked horizon. Our results show that over the studied range of experimental conditions, growth rate has no effect on the boron isotopic composition of calcite (even if it is difficult to have a

definitive statement due to the reproducibility of the $\delta^{11}B$ SIMS measurements), and that in contrast, boron partition coefficients can be substantially influenced by growth rate. The relationship between D_B and V could be explained with growth entrapment model (GEM, see Discussion section for details). A key aspect of our study is that the range of observed growth rates for calcite crystals we synthesized (between 0.04-0.13 nm/s) overlaps with values reported for naturally occurring $CaCO_3$ (0.006-3.3 nm/s) in benthic foraminifera (Kuile and Erez, 1984), coccolithophorids (Stoll et al., 2002), scallops (Owen et al., 2002), and speleothems (Baker et al., 1998), making these results of potential relevance to boron-based proxies in these types of carbonate, and related forms.

2. EXPERIMENTAL AND ANALYTICAL METHODS

2.1. **Calcite precipitation**

The calcite growth method used was adapted from previously developed approaches (Gruzensky 1967; Paquette and Reeder 1995). We modified this precipitation method by the introduction of sub-sampling and by using multiple REE spikes to constrain growth rates. The initial solution was prepared by dissolving NH_4Cl in deionized (DI) H_2O to achieve a concentration of 0.5 mol/l, along with minor amounts of reagent grade $CaCl_2{\cdot}2H_2O$ (0.01 mol/L), $MgCl_2{\cdot}6H_2O$ (10^{-3} mol/L), $SrCl_2{\cdot}6H_2O$ (10^{-4} mol/L), $BaCl_2{\cdot}2H_2O$ ($2{\cdot}10^{-5}$ mol/L), $LiOH{\cdot}H_2O$ ($5{\cdot}10^{-4}$ mol/L), H_3BO_3 (0.01 mol/L), and a U ICP-MS standard (10^{-5} mol/L). The salinity and ionic strength of the fluid (29.4 and 0.58, respectively) were calculated from concentrations of the salts. The pH of the solution was initially adjusted to 5.5 (NBS-scale) by addition of reagent grade NaOH to achieve an initial pH similar to what was reported by Paquette and Reeder (1995). Two liters of

solution were transferred into closed Pyrex flask connected to a glass vial containing ammonium carbonate (see Figure 1 in Gabitov and Watson, 2006; Gabitov et al., 2014). Calcite crystals grew by diffusion of CO_2 from slowly decomposing ammonium carbonate. In order to encourage the growth of crystals that would be large enough for SIMS analysis, the fluids were not stirred during calcite precipitation except after the addition of each REE spike, when the solutions were mixed by repeated injection and withdrawal of fluid using a 60-ml syringe. The calcite sample analyzed in this study is the same as the one described in Gabitov et al. (2012 and 2014).

REE spikes (Sm, La, Nd, and Tb) were sequentially introduced into the growth medium by the addition of a 1 ml aliquot of dilute REE-bearing fluid, which yielded an estimated REE concentration range in the final solution ranging from 0.1 to 0.5 ppb. The first REE spike (Sm) was introduced into the solution as soon as calcite crystals became visible with naked eye. Therefore the onset of nucleation was not determined directly, but was estimated from the time interval between two visual observations (no crystals visually apparent, and crystals visually apparent). The second spike (La) was introduced after 24 days, followed by a third (Nd) spike after 35.8 days, and a final (Tb) spike after 85.9 days (Table 1).

In total, the entire time that elapsed during which calcite precipitated was 149.9 days. Fluids were sampled periodically for measurement of pH, and stored in a refrigerator for future measurements. Solution pH was immediately determined after collection of the fluid using a OAKTON pH 510 meter with an "All-in-One" pH/Temp electrode calibrated using 7.00 and 10. pH values are all reported on the NBS-scale. We

observed that pH slowly increased during calcite precipitation from values of 7.96±0.06 to 8.17±0.02 (Table 1, supplemental Fig. S-1).

2.2. **Analyses of fluids**

Analyses to determine calcium and boron concentrations in the fluids were performed using a Varian VISTA PRO, an inductively-coupled optical emission spectrophotometer (ICP-OES) at the School of GeoSciences at the University of Edinburgh, and a Thermo Element XR ICP mass spectrometer (ICP-MS) at the Department of Earth Sciences in the University of Cambridge. The analytical precision was assessed using the standard deviations of in-house reference solutions was ~2% for both measurements (1σ), for more details about measurement see (Greaves et al., 2005 and Misra et al., 2014).

Dissolved inorganic carbon (DIC) concentrations were determined using a coulometric Single-Operator Multi-Metabolic Analyzer (SOMMA) system in the Biogeochemistry Laboratory at the University of California, Los Angeles (UCLA) (for details see Johnson et al., 1993). Routine analysis of seawater certified reference materials (CRMs, produced by Andrew Dickson, Scripps Institution of Oceanography) were used to assess the accuracy of DIC data. Based on 149 comparisons with the CRMs, the accuracy of the method has been determined to be ± 2.1 µmol/kg.

2.3. In situ analyses of calcite

2.3.1. Sample preparation

Calcite mineralogy was confirmed by X-ray diffraction (XRD) analyses in the Institute for Imaging & Analytical Technologies (i^2AT) at Mississippi State University

(MSU). The largest calcite crystal was mounted in epoxy (EpoxiCure®, Buehler) in such a way that the pyramid base (the crystal side adjacent to the substrate during growth) was exposed for SIMS measurements. The mount was polished down using a 1-µm size diamond paste and the crystal was analyzed on the CAMECA ims 1270 ion microprobe at UCLA (Los Angeles, USA), first to determine Ca and REE concentrations, and subsequently for Ca and B concentrations. $\delta^{11}B$ and B concentrations were determined in Centre de Recherches Pétrographiques et Géochimiques (CRPG-CNRS, Nancy, France), also using a CAMECA ims 1270 ion microprobe. In order to quantify SIMS determinations, the raw $^{11}B^+/^{40}Ca^{++}$ and $^{11}B^+/^{10}B^+$ ratios for samples were normalized to those of a calcium carbonate in-house reference material with known compositions ([B]=22±3 ppm, $\delta^{11}B$=21±1 ‰; Rollion-Bard et al, 2003).

2.3.2. Further details of Ca and B analyses by SIMS

Following REE determinations, the mount was polished to remove about 4 µm of calcite and analyzed for B/Ca at the same x-y coordinates used for REE measurements (see Gabitov et al. 2012 for details). Because of the re-polishing, a small shift (<4 µm) in x-y coordinates is possible, which is insignificant relative to the size of the ion beam (~30 µm). Calcium and boron abundances were measured with a 70 nA $^{16}O^-$ primary beam at 30-40 µm lateral dimensions on the sample surface. Positive secondary ions corresponding to masses corresponding to the background (mass 9.8), $^{11}B^+$, and $^{40}Ca^{++}$ were measured at a mass resolving power of ~3000 and in monocollection mode with an electron multiplier (EM). The typical internal error, i.e. the standard error of one single analysis, was ± 0.4 %. Reproducibility of $^{11}B^+/^{40}Ca^{++}$ ratios on a carbonate reference

material (WP22, Rollion-Bard et al, 2003) was 10% (1σ, n=10). The homogeneity of this in-house reference material was checked for B/Ca and $\delta^{11}B$ values by multiple measurements in another study (Rollion-Bard, 2010).

2.3.3. *Further details of $\delta^{11}B$ analyses by SIMS*

The method used for SIMS $\delta^{11}B$ analyses was the same than described in Blamart et al. (2007) and Rollion-Bard and Erez (2010). Measurements were made with a 70 nA $^{16}O^-$ primary beam that had a lateral dimension of 30-40 µm at the sample surface. The positive secondary ions $^{10}B^+$ and $^{11}B^+$ were measured with a mass resolving power of ~3000 in monocollection mode using an electron multiplier detector. The typical intensities in the sample for $^{11}B^+$ were between ~$5 \cdot 10^3$ counts per second (cps) and $18 \cdot 10^3$ cps. Each analysis consists of 50 cycles of 10 s for $^{10}B^+$ and 6 s for $^{11}B^+$. The typical internal error, calculated from the standard deviation of one single analysis divided by the square root of 50 cycles (i.e. $\sigma/\sqrt{50}$), was ± 0.5 ‰. The average external error, as estimated by multiple measurements of the reference material, was ± 2 ‰ (2σ, n=10). Thus the total error for each analysis is ≈2.2 ‰ (2σ, with $\sigma = \sqrt{(\sigma_{int}^2 + \sigma_{ext}^2)}$, σ_{int} being the internal error and σ_{ext} being the external reproducibility).

During the same session that $\delta^{11}B$ was measured, the B content was estimated from the emissivity of boron (i.e. cps/nA/ppm) as determined on the reference material and used to convert the measured boron intensities into ppm. This method is not as precise as the direct measurement of B/Ca ratios described in the previous section, and our reproducibility for this ratio, based on multiple measurements of the reference in-house

material, was about ±20 % (1σ, n=10). As more accurate and precise B/Ca ratios were obtained from the direct measurements of $^{11}B^{+}$ and $^{40}Ca^{++}$, we corrected the estimates of B content derived from emissivity measurements (corresponding to cps/nA/ppm) to agree with the more-precise direct analyses of $^{11}B^{+}/^{40}Ca^{++}$ from the measurements performed in the same part of the calcite crystal. We thus obtained a correcting factor that was applied for all the values of B/Ca calculated from the boron emissivity.

3. RESULTS

3.1. **B and Ca composition of the fluids**

The boron concentration of the fluids that were initially sampled was 56 ppm; it decreased after the onset of crystallization and remained near constant during the experiment ([B]=42 ppm; s.e. of 0.4 ppm, n = 4 samples of fluid). This initial decrease in B_{fluid} did not affect our B partitioning data, because D_B was calculated for calcite precipitated during near constant B content in the fluid. Over the course of the run, Ca concentrations decreased in the solution from 327 ppm to 95 ppm. The evolution of B/Ca (mol/mol) in the fluid over the course of the experiment can be fitted by the following linear function (Fig. 2b):

$$B/Ca=5.7\cdot10^{3}t+0.675, \quad r^{2}=0.98 \qquad \text{(eq. 1)}$$

where t is the duration of the experiment in days assuming that t=0 at the addition of Sm spike.

The concentrations of carbonate species were calculated using an excel implementation of CO2SYS and measured pH and DIC values (Lewis and Wallace, 1998). The initial fluid had low DIC and $[CO_3^{2-}]$ values, which are assumed to have

increased to unknown amounts before the onset of crystallization due to the continuous supply of CO_2. After precipitation was visually identified as having started, we observed that both DIC and $[CO_3^{2-}]$ values continued to increase (Table 1). Not all of the fluid samples were analyzed for DIC because of the design of the coulometric system, which required 150 ml of fluid for a single analysis. Fluid saturation state with respect to calcite (Ω) was defined as $[Ca^{2+}]\cdot[CO_3^{2-}]/K^*_{sp}$. K^*_{sp} is the stoichiometric solubility constant of calcite in seawater determined from the relationship developed by Mucci (1983), with a pK^*_{sp} of 6.46 at the temperature and salinity values corresponding to our experiment (24.6°C and 29.4).

3.2. **B content and $\delta^{11}B$ of the calcite crystal**

In order to investigate growth rate controls on boron isotopic and elemental partitioning, REE spikes were used to quantify V. The crystal zones defined by the REE spikes are shown in Fig. 1. The sequential appearance of the different REE reflects the order of their addition into the fluid of precipitation (i.e., starting with Sm and ending with Tb). Growth rates were determined as the width of each zone (Δx) in each profile divided by the time between REE spikes (Δt). Values of growth rates in the crystal interiors are higher than at the edges - that is, V decreased from 0.133 to 0.038 nm/s in the Sm-La and Nd-Tb zones, respectively.

SIMS profiles show the B distribution within a crystal (Fig. 2). Boron data collected in calcite that grew only after the addition of the REE spikes were used to study boron partitioning between the mineral and fluid. One data point was excluded - the datum marked with “X” on Fig. 2, which was likely affected by rapid crystallization

(details are discussed further below). The additions of small amounts of REE (≤0.5 ppb) to the fluid have unlikely affected the B incorporation into calcite.

We calculated values for the boron partition coefficient, D_B. $D_B = B(t)_{calcite}/B_{fluid}$, where $B(t)_{calcite}$ was determined using the average value of measurements from multiple SIMS spots in a particular REE-spiked zone in the calcite crystal, with uncertainties reported as the standard error (1 s.e.) of these data. Error bars reported for V represent the 1 s.d. determined using estimates of V from opposite sides of the crystal for a particular REE spiked zone. Values of D_B increased by a factor of ≈2 (from 0.5 to 0.9) associated with an increase in V by a factor of ≈3 (from 0.04 to 0.13 nm/s) (Table 3 and Fig. 3). B in marine carbonates is often expressed as B/Ca, therefore we also calculated the exchange coefficient $K_{B/Ca}$ as $(B/Ca_{calcite})/(B/Ca_{fluid})$. $K_{B/Ca}$ increased from $1.77 \cdot 10^{-4}$ to $4.76 \cdot 10^{-4}$ with increasing of growth rate from 0.038 to 0.13 nm/s (Table 3), and this trend is similar to the one observed for D_B despite the evolution of [Ca] in the fluid during the experiment.

Both B content, $K_{B/Ca}$, and D_B increase from the edge of the REE-spiked calcite crystal toward its interior. In addition, V changes in this region. However, a dip in B content was observed within the ~600 µm REE-free area around the center of the crystal (Fig. 2 and Table 2). The growth rate of this central zone was estimated to be higher or equal to 0.23 nm/s (Gabitov et al. 2012), confirming a decrease of V during crystal growth.

In contrast, $\delta^{11}B$ ratios are invariant across the calcite crystal within analytical error at the 2σ level, with average values of ≈-9.3±1.3 ‰ (Table 2). The $\delta^{11}B$ of fluids was not determined, and so we cannot elaborate on the significance of this result with respect

to isotopic fractionation between the mineral and fluid. It is possible the data indicates there no dependence on growth rate of boron isotopic fractionation between fluid and calcite; although data for fluids are required to ensure that competing effects are not being masked by examining data for the crystal in isolation.

3.3. **Topography of a single crystal**

The synthetic calcite crystals were characterized with SIMS traverses from the crystal center to the edge using spot profiles. Kita et al. (2009) suggested that there are minor topographic effects when surface relief after polishing is less than 1 µm. To verify that topographic effects could be the cause of B/Ca ratios decrease from centre to the edges of the crystal, we performed imaging with an interference microscope (PHASE SHIFT MicroXAM Surface Mapping Microscope Crystal). This imaging revealed the presence of slight relief on the sample surface, with calcite edges elevated by 0.6 to 0.9 µm above the crystal centers. Similar relief of less than 1 µm was noted on the standard grains (i.e. carbonate in-house reference material grains used in this study). All crystals examined were located within ~7 mm of the center of the epoxy mount to avoid any X-Y effect as described in Kita et al. (2009). Taken together, this evidence indicates that the depleted B/Ca values at the edges of our experimental crystal are not an analytical artifact.

4. DISCUSSION

4.1. **B content of the calcite crystal**

There are two potential scenarios that could explain the observed depletion of boron in the crystal center: 1) an increase of fluid boron/DIC ratios during initial crystallization, before the addition of the first REE spike, and 2) the formation of a distinct fluid boundary layer adjacent to the calcite surface associated with fast growth rates in REE-free zone.

In the first scenario, calcite nucleation that is followed by a rapid crystallization will lead to the rapid consumption of carbon from the fluid. As a consequence, at the beginning of crystal growth, fluid B/DIC ratios increase. Subsequent reductions in values for V reflect more balanced fluxes of carbon into and out of solution – i.e., a better balance between the diffusion of CO_2 from ammonium carbonate, and the consumption of DIC by growing crystals. High growth rates would have likely completely entrapped composition of chemically anomalous layer near the surface of the crystal (i.e., yielded 100% of surface entrapment resulting in D_B=const (see Discussion section for details of GEM). Therefore mineral boron/carbon ratios would depend entirely on fluid B/DIC ratios during any rapid precipitation that occurred, including prior to the introduction of the REE spikes. Similar phenomenon was observed for Sr/Ca distribution in fast grown calcite (Gabitov et al. 2014).

A second possible explanation for the depleted boron contents near the cores of the crystals relates to the presence of a fluid boundary layer. When values of V are greater than 10 nm/s, a diffusive boundary layer between calcite surface and the fluid will develop. Our estimates of crystal growth rates for growth during the experiment when REE spikes were used are less than this value. However values of V could have been high enough for the formation of a solution boundary layer during the period prior to the

addition of the REE spikes, but during and after calcite nucleation began, and thus could have caused depletions in boron abundance in the core of the crystal. The presence of a solution boundary layer should affect B concentrations of the crystal when mineral growth rates are rapid and where ions diffusivities are $\approx 10^9$ nm^2/s (Smith et al.; 1955; Li and Gregory, 1974; Watson and Müller, 2009).

These two scenarios could in fact be linked to each other because rapid crystallization could lower carbon concentrations not only in the whole/bulk reservoir but also at the boundary between the growing calcite crystal and the fluid. Another factor that may be important relates to the possible formation of amorphous calcium carbonate (ACC) during the initial stages of calcite crystal growth, as boron may be partitioned into ACC differently than calcite. ACC formation is possible at the beginning of our precipitation experiments as the initial apparent solubility product ($Ca^{2+} \cdot CO_3^{2-}$) could have been higher than the threshold between formation of calcite and ACC ($9.21 \cdot 10^{-7}$ mol^2/kg^2) calculated from relationships reported by Clarkson et al. (1992) at 24.6°C. Although there is no direct evidence for the presence of ACC (according XRD analyses), fluids sampled after the addition of REE yielded $Ca^{2+} \cdot CO_3^{2-}$ values ranging from 6.66 to 9.30 mol^2/kg^2. It is also possible that the addition of REE spikes to the fluids could have affected D_B, triggering an interaction between B and REE-containing species at the calcite surface. However, it is unlikely that the addition of the first REE-containing spike (bearing Sm) into fluids caused a rapid increase of D_B by interacting with B, as the addition of subsequent REE spikes did not apparently influence D_B. Furthermore, another study has shown that SIMS-based profiles of crystals that contain REE in their centers,

and those without, do not differ from each other. This study examined Sr partitioning into calcite and yield similar profiles to B (Gabitov et al., 2014).

4.2. Partition coefficient and growth rate

The observed relationship between D_B (or $K_{B/Ca}$) and growth rate is similar to what has previously been reported from studies of Sr and Ba incorporation into calcite (Lorens 1981; Tesoriero and Pankow 1996; Gabitov and Watson 2006; Tang et al. 2008a; Gabitov et al. 2014), even if these elements are cations whereas B is thought to incorporate into calcite at the site of CO_3^{2-}. These two elements show a significant positive correlation between partition coefficients and growth rate. The change in pH during the experiment (from 7.96±0.06 to 8.17±0.02) cannot explain the observed D_B-V trend, but could explain, some of the observed scatter in the $\delta^{11}B$ data. The increase in pH should result in an increase in $\delta^{11}B$ of ~2.3 ‰, using the experimental curve for borate reported by Klochko et al. (2006) and assuming that only borate ions incorporate into calcite (Hemming and Hanson, 1992). Unfortunately we cannot state about this possible increase of $\delta^{11}B$ values due to the analytical uncertainty (≈2.2 ‰, 2σ).

The lack of information on calcite precipitation rate for the experiments of Hemming et al. (1995) precludes direct comparison of their D_B data to ours. Hemming et al. (1995) grew calcite at 20°C, pH=8.03±0.07, B_{fluid}=44 ppm, and Ca_{fluid}=5370 ppm. The high Ca_{fluid} and hence Ω suggest that their calcites grew at faster rates than the crystals grown for our study. The growth rates determined in our study (0.04-0.13 nm/s) overlap with the slowest step velocities of crystal face $\{10\bar{1}4\}$ (0.1-0.4 nm/s) grown from solutions with high Ca content (920-3690 ppm) (Reeder 1996). Our D_B values of 0.5 to 0.9 are lower

than those from Hemming et al. (1995), which yielded a D_B of 3.1. Therefore it is possible that the large D_B reported by Hemming et al. (1995) could be explained by higher growth rates in their experiments and are consistent with the observed D_B-V trend in our study (Figure 3).

We compared our extension velocities with the bulk precipitation rate (R) of individual crystal. Mean "reactive" surface area (A_{REE} in m^2) for each REE-spiked zone of our individual crystal was calculated by considering that the shape is spherical. This assumption is reasonable because of the large error in the surface area estimate, which exceeds the A_{REE} difference if we assumed the crystal shape was a sphere or a rhombohedron. We also calculated the volume and amount of calcite precipitated during each interval between REE spikes. The bulk precipitation rate for each REE-spiked layer was determined as $R_{Sm\text{-}La}$ = $calcite_{Sm\text{-}La}$ / $A_{Sm\text{-}La}$ / $\Delta t_{Sm\text{-}La}$ [$\mu mol/m^2/h$]. An example for Sm-La zone is shown here for the mean specific surface area of an individual crystal grown between addition of Sm and La spikes of $(2.1\pm0.43)\cdot10^{-3}$ m^2/g. This value is much lower than those determined in experiments with small calcite crystals (size<10 μm, 0.52 m^2/g, Zhong and Mucci 1989). The relationship between V and R was determined in our work and can be described by the following empirical equation:

$$\log V = 1.01\cdot\log(R) - 5.0,\ r^2 = 0.84 \qquad \text{(eq. 2)}$$

To confirm the validity of equation-2, V was calculated using values of R reported by Tesoriero and Pankow (1996). In their experiments, a thin layer of calcite was precipitated on seed material with a size of 5-10 μm, a specific surface area of 0.6 m^2/g, log(R)=0.2-2.6 nmol/mg/min or 2.2-4.6 $\mu mol/m^2/h$, and an experimental duration of 0.095-56 h (with slower precipitation rates corresponds to the longer duration).

Substitution of their log(R) values into equation-2 yielded to V=0.0017-0.47 nm/s, which corresponds to a precipitation width of 161-339 nm on the seeds. This thickness of new grown calcite would increase the "reactive" surface area by 3.2-6.9 % (m^2), which is consistent with reported <10 % change (Tesoriero and Pankow 1996; Zhong and Mucci 1989).

4.3. Application of GEM to experimental data

In our work we focus on V because growth velocity is more appropriate for modelling using the growth entrapment model (GEM). A positive correlation between D_B and V is predicted by GEM, a model that was successfully used to explain observations of disequilibrium in minor elements, as well as oxygen and calcium isotopes fractionation between carbonate minerals and fluid (Stoll et al., 2002; Gabitov and Watson, 2006; Gaetani and Cohen, 2006; Gabitov et al., 2008; Tang et al., 2008a,b; Gabitov et al., 2012; Saulnier et al., 2012; Gabitov, 2013). GEM describes disequilibrium fractionation of elements and isotopes between a crystal and its growth medium as a consequence of the "capture" of a chemically anomalous solid near-surface region of the lattice during crystal growth (Watson and Liang, 1995; Watson, 1996, 2004). The anomalous layer owes its existence at least in part to relaxation from normal lattice positions of atoms located within ~1 nm of the surface (see Fenter et al. 2000; Rohl et al. 2003). Watson and co-workers consider that equilibrium fractionation between crystals and their growth media can occur only when solid-state diffusion in the near-surface region (D_s) dominates over V. A premise of GEM is that D_s is much faster than diffusion in the crystal lattice (D_l) ($D_s \approx 10^{16} D_l$). This large diffusivity difference is consistent with the results of

cadmium uptake in calcite from the work of Stipp et al. (1992). If growth rates are sufficiently high, then V dominates over D_s and the anomalous surface is archived (at least partially) in the overall composition of the crystal. If D_s is completely ineffective during growth, the composition of the resulting crystal differs from the equilibrium composition by the factor F (the partition coefficient between the near-surface region and the crystal lattice).

A numerical simulation of our experimental data is presented in Fig. 4. The simulations were conducted using the new version of GEM (GEM2) running with QuickBASIC (QB64) code. The description of the model is presented in detail by Watson (2004), where he considered that concentration (C) changes as a function of the distance from the surface of the crystal:

$$C(x) = C_{eq} \cdot F^{\exp(x/l)} \qquad \text{(A1.1)}$$

where $C(x)$ is the concentration of the impurity (i.e. element other than Ca, C, or O) in the crystal at some distance x from the surface, C_{eq} is the concentration reflecting partition equilibrium between the growth medium and the bulk crystal, F is the surface enrichment factor (i.e. the ratio of B between crystal near-surface region and its lattice) and l (0.5 nm) is the half-thickness of the enriched surface layer. The enrichment factor (F) was taken as the ratio of their maximum to minimum D_B values, i.e. 3.1/0.11=28.1 from the works of Hemming et al. (1995) and Hemming et al. (1998) respectively.

The diffusivity of B into the calcite lattice (D_l^B) was assumed to be much lower than in the near-surface region. In the model, the value of D_l becomes less important as $D_l << D_s$. For example, at V=0.1 nm/s, changing D_l from 10^{-18} to 10^{-35} affects D_B / D_{eq}^B by

less than 2%. The parameters of D_s and distance multiplier (m) were optimized to obtain the best fit of B experimental data from this study (D_s=0.06 and m=∞). An infinite m signifies that the diffusivity is independent of depth in the crystal (and equal to D_s) over a distance much greater than the thickness of the compositionally distinct near-surface layer.

Simulations indicate that at growth rates of less than 0.03 nm/s, D_B becomes less dependent on growth rate and approaches equilibrium values when $V<10^{-3}$ nm/s. The value of D_B during equilibrium lattice-fluid partitioning (D_B^{eq}) is less than 0.5. Simulations show that D_B increases rapidly as values of V go from 0.03 to 3 nm/s. Over this range of growth rates, D_B is predicted to be correlated with V: at slow growth rates, simulated values of D_B reflect the minimum capture of B from the near-surface region of calcite; at faster growth rates, more surface entrapment of B from the anomalous region occurs. The model indicates that when V is greater than 10 nm/s, complete or 100% surface entrapment occurs and D_B values are 3.1, representing complete disequilibrium partitioning of B between calcite and fluid.

Surface entrapment could explain the enrichment of B in the slow growth equivalent vicinal faces (a′ and b′) observed by Hemming et al. (1998), through the difference in F and D_s between non-equivalent face pairs. To test whether growth rate and the GEM model might explain the data from Hemming et al. (1998), we conducted a simulation. Note that the experimentally-determined growth step velocities determined by Reeder (1996) and applied to the data of Hemming et al. (1998) are within the range of values for V used above in our GEM simulations. For these new calculations, we set the F value to 16.9. This value was determined to be the ratio between the published

maximum B content measured *in situ* in a′-b′ (82.1 ppm) and minimum B content in a′-b′ vicinals (4.86 ppm) (Table 1, Hemming et al. 1998). To determine V, we used constraints from Reeder (1996), who reported the growth step velocity of face a′ ($V_{a'-b'}$) is equal to V_{a-b} /15. Therefore variation in $V_{a'-b'}$ from 10^{-4} to 1 nm/s corresponds to a V_{a-b} change from $1.5 \cdot 10^{-3}$ to 15 nm/s. In our model calculations, boron diffusivities in the near surface layer were set to $D_{s(a'-b')}$= 0.003 and $D_{s(a-b)}$= 0.3 nm^2/s for a′-b′ and a-b respectively. Values for the other parameters (D_B^{eq}, D_l, l, and m) were identical to our previous simulations (Fig. 5).

The simulations show that the change in enrichment factor F is unlikely an explanation for the reported boron enrichment in a′ and b′ from Hemming et al. (1998) because a smaller kink site would discriminate against boron incorporation into the a′-b′ faces, relative to the a-b faces. Model results also indicate that fast near-surface diffusion would cause boron depletion in rapidly growing a-b faces, relative to slower growing a′-b′ faces. The difference in D_s (by two orders of magnitude) could explain the affinity of boron to slower grown vicinal faces (a′-b′), with a maximum $D_{B(a'-b')}/D_{B(a-b)}$ = ~2.8 when $V_{(a'-b')}=V_{(a-b)}/15$ = ~0.01 nm/s. An important caveat to note is that growth step velocities of vicinal faces on calcite crystals are different from V, as we relied on crystal extension rates without distinguishing between the geometry of the faces.

Another essential factor to be considered is that B partitioning could also be species dependent. In that case, the simulations may be overly simplified. If B partitioning was species-dependent, we might expect to see a relationship between boron isotope fractionation and growth rate. We do not see any evidence from the mineral $\delta^{11}B$ data

alone for a growth rate effect. However fluid $\delta^{11}B$ data from our experiments is lacking, precluding our determination of mineral-fluid fractionation factors as a function of growth rate and the uncertainty in $\delta^{11}B$ can hinder any interpretation on effect of growth rate. Nevertheless, we can note that, if there is an effect on $\delta^{11}B$, this effect must be <4 ‰ (corresponding to our 2σerror). Although further work needs to be done, these results indicate that variations in growth rate are a factor that can influence B/Ca ratios measured in biogenic carbonates. This could, in part, explain the scattering data of calibration between B/Ca and $[B(OH)_4^-]/[HCO_3^-]$ in a single species of foraminifera (Yu et al, 2007a,b).

5. CONCLUSIONS

Our *in situ* study of synthetic calcite provides the first evidence that boron partitioning between calcite and fluid increases with crystal growth rate over the range of growth rates investigated in this study (0.038-0.13 nm/s). The dependence of D_B (or $K_{B/Ca}$) with growth rate can be explained using the growth entrapment model, with equilibrium values attained at low growth rates, and the near surface region of calcite enriched in boron relative to the lattice at equilibrium. A growth rate effect on boron partitioning into carbonate minerals could explain the variety of relationships between B/Ca ratios and carbonate system parameters determined for foraminifera and other types of biogenic calcite (e.g., Yu and Elderfield, 2007; Yu et al, 2007a,b; Dawber and Tripati, 2012). No discernable change in $\delta^{11}B$ was observed in calcite grown at variable growth rates, although a lack of data on fluid composition precluded determination of fractionation factors.

Acknowledgments. We would like to thank Axel Schmitt, Kevin McKeegan, and Mark Harrison for their help and support with the ion microprobe measurements. Experiments and SIMS analyses were supported by NSF EAR, Instrumentation and Facilities. We are grateful to Walter Geibert, Mervyn Greaves, Sambuddha Misra, and Harry Elderfield for support of elemental measurements at the University of Edinburgh and the University of Cambridge. We thank Anita Leinweber for measuring DIC; these analyses were covered by ETH grant no. 4 443869-AL-20600, ARC-1215551), by the INSU program (INTERRVIE), by DOE BES award DE-SC0010288, and by a Hellman Fellowship. Elemental measurements of fluids were also covered by ERC grant NEWLOG 267931 to H. Elderfield. We also thank MSU and i^2AT for supporting XRD analyses. The authors are grateful to Bruce Watson for providing the code used to model growth entrapment.

References

Adkins J. F., Boyle E. A., Curry W. B. and Lutringer A. (2003) Stable isotopes in deep-sea corals and a new mechanism for "vital effects". *Geochim. Cosmochim. Acta* **67**, 1129-1143.

Allen K.A., Hönisch B., Eggins S.M. and Rosenthal Y. (2012) Environmental controls on B/Ca in tests of the planktic foraminifer species *Globigerinoides ruber* and *Globigerinoides sacculifer*. *Earth Planet. Sci. Lett*. **350-351**, 270-280.

Baker A., Genty D., Dreybrodt W., Barnes W.L., Mockler N.J., and Grapes J. (1998) Testing theoretically predicted stalagmite rate with recent annually laminated samples: Implications for past stalagmite deposition. *Geochim. Cosmochim. Acta*, **62**, 393-404.

Blamart D., Rollion-Bard C., Meibom A., Cuif J.P, Juillet-Leclerc A., Dauphin Y. (2007) Correlation of boron isotopic composition with ultrastructure in the deep- sea coral *Lophelia pertusa*: Implications for biomineralization and paleo-pH. *Geochem. Geophys. Geosys.*, Q12001, doi:10.1029/2007GC001686.

Clarkson J.R., Price T.J., and Adams C.J. (1992) Role of Metastable Phases in the Spontaneous Precipitation of Calcium Carbonate. *J. Chem. Soc. Faraday Trans. J.*, **88**, 243-249.

Dawber C. and Tripati A. (2012) Relationship between bottom water carbonate saturation and X/Ca in core-top samples of the benthic foraminifera *Oridorsalis umbonatus*, *Biogeosciences,* **9**, 3029-3045.

Gabitov R.I. and Watson E.B. (2006) Partitioning of strontium between calcite and fluid. *Geochem. Geophys. Geosys.* **7**, Q11004, doi:10.1029/2005GC001216.

Gabitov R. I., Gaetani G. A., Watson E. B., Cohen A. L. and Ehrlich H. L. (2008) Experimental determination of temperature and growth rate effects on U^{6+} and Mg^{2+} partitioning between aragonite and fluid. *Geochim. Cosmochim. Acta*, **72**, 4058–4068.

Gabitov R.I., Watson E.B., and Sadekov A. (2012*)* Oxygen isotope fractionation between calcite and fluid as a function of growth rate and temperature: An in situ study. *Chem. Geol.*, **306–307**, 92-102.

Gabitov R.I., Sadekov A., and Leinweber A. (2014) Crystal growth rate effect on Mg/Ca and Sr/Ca partitioning between calcite and fluid: An in situ approach. *Chem. Geol.* (doi:10.1016/j.chemgeo.2013.12.019.

de Nooijer L.J., Toyofuku T., and Kitazato H. (2009) Foraminifera promote calcification by elevating their intracellular pH. *PNAS*, **106**, 15374 –15378.

Gaetani G.A. and Cohen A.L. (2006) Element partitioning during precipitation of aragonite from seawater: A framework for understanding paleoproxies. *Geochim. Cosmochim. Acta*, **70**, 4617-4634.

Gattuso J.-P. and Hansson L. (2011) Ocean acidification. Eds Gattuso J.-P. and Hansson L., Oxford University Press. 352 pp.

Gruzensky P.M. (1967) Growth of calcite crystals. *J. Phys. Chem. Solids,* S **1**, 365-367.

Fenter P., Geissbuhler P., Dimasi E., Srajer J., Sorensen L.B., and Sturchio N.C. (2000) Surface speciation of calcite observed in situ by high-resolution X-ray reflectivity. *Geochim. Cosmochim. Acta*, **64**, 1221-1228.

Johnson K. M., Wills K. D., Buttler D. B., Johnson W. K. and Wong C. S. (1993) Coulometric total carbon dioxide analysis for marine studies: maximizing the performance of an automated gas extraction system and coulometric detector. *Mar. Chem*., **44**, 167-187.

Hemming N.G. and Hanson G.N. (1992) Boron isotopic composition and concentration in modern marine carbonates. *Geochim. Cosmochim. Acta*, **56**, 537-543.

Hemming N.G., Reeder R.J., and Hanson G.N. (1995) Mineral-fluid partitioning and isotopic fractionation of boron in synthetic calcium carbonate. *Geochim. Cosmochim. Acta*, **59**, 371-379.

Hemming N.G., Reeder R.J., and Hart S.R. (1998) Growth-step-selective incorporation of boron on the calcite surface *Geochim. Cosmochim. Acta*, **62**, 2915-2922.

Hershey J. P., Fernandez M., Milne P. J. and Millero F. J. (1986) The ionization of boric acid in NaCl, Na-Ca-Cl, and Na-Mg-Cl solutions at 25 °C. Geochim. Cosmochim. Acta, **50**, 143-148.

Hobbs M.Y. and Reardon E.J. (1999) Effect of pH on boron coprecipitation by calcite: Further evidence for nonequilibrium partitioning of trace elements. *Geochim. Cosmochim. Acta*, **63**, 1013-1021.

Hönisch B., Hemming N. G.n Grottoli A. G., Amat A., Hanson G. N. and Bijma J. (2004) Assessing scleractinian corals as recorders for paleo-pH: Empirical calibration and vital effects. *Geochim. Cosmochim. Acta* **68**, 3675-3685.

Kita N.T., Ushikubo T., Fu B., Valley J.W. (2009) High precision SIMS oxygen isotope analysis and the effect of sample topography. *Chem. Geol.,* **264**, 43–57.

Klochko K., Kaufman A. J., Yao W., Byrne R. H. and Tossell J. A. (2006) Experimental measurement of boron isotope fractionation in seawater. *Earth Planet. Sci. Lett*., **248**, 261–270.

Kuile B. and Erez J. (1984) In-situ growth rate experiments on the symbiont bearing foraminifera *Amphistegina lobifera* and *Amphisorus hemrprichii*. *J. Foram. Res*., **14**, 262-276.

Lewis E. and Wallace D.W.R., 1998. Program developed for CO2 system calculations. Carbon Dioxide Information Analysis Center, Oak Ridge National Laboratory. U.S Department of Energy, Oak Ridge, Tennessee.

Li Y.-H. and Gregory S. (1974) Diffusion of ions in sea water and in deep-sea sediments. *Geochim. Cosmochim. Acta*, **38**, 703–714.

Lorens R.B. (1981) Sr, Cd, Mn, and Co distribution coefficients in calcite as a function of calcite precipitation rate. *Geochim. Cosmochim. Acta*, **45**, 553-561.

McConnaughey T. (1989) ^{13}C and ^{18}O isotopic disequilibrium in biological carbonates: II. In vitro simulation of kinetic isotope effects. *Geochim. Cosmochim. Acta* **53**, 163-171.

Misra S., Greaves M., Owen R., Kerr J., Elmore A. C., Elderfield H. Determination of B/Ca of Natural Carbonates by HR-ICP-MS. Geochemistry, Geophysics, Geosystems. under review nov. 2013

Mucci A. (1983) The solubility of calcite and aragonite in seawater at various salinities, temperatures, and one atmosphere total pressure. *Am. J. Sci.*, **283**, 780–799.

Orr J. C., Fabry V. C., Aumont O., Bopp L., Doney S. C., Feely R. A., Gnanadesikan A., Gruber N., Ishida A., Joos F., Key R. M., Lindsay K., Maier-Reimer E., et al. (2005) Anthropogenic ocean acidification over the twenty-first century and its impact on calcifying organisms. *Nature*, **437**, 681-686.

Owen R., Kennedy H., and Richardson C. (2002) Isotopic partitioning between scallop shell calcite and seawater: Effect of shell growth rate. *Geochim. Cosmochim. Acta*, **66**, 1727-1737.

Pagani M., Lemarchand D., Spivack A. and Gaillardet J. (2005) A critical evaluation of the boron isotope-pH proxy: The accuracy of ancient ocean pH estimates. *Geochim. Cosmochim. Acta* **69**, 953-961.

Paquette J. and Reeder R.J. (1995) Relationship between surface structure, growth mechanism, and trace element incorporation in calcite. *Geochim. Cosmochim. Acta*, **59**, 735–749.

Palmer M. R., Pearson P. N. and Cobb S. J. (1998) Reconstructing past ocean pH-depth profiles. *Science* **282**, 1468-1471.

Pearson P. N. and Palmer M. R. (2000) Atmospheric carbon dioxide concentrations over the past 60 million years. *Nature* **406**, 695-699.

Rae J. W. B., Foster G. L., Schmidt D. N. and Elliott T. (2011) Boron isotopes and B/Ca in benthic foraminifera: Proxies for the deep ocean carbonate system. *Earth Planet. Sci. Lett.* **302**, 403-413.

Reeder R.J. (1996) Interaction of divalent cobalt, zinc, cadmium, and barium with the calcite surface during layer growth. *Geochim. Cosmochim. Acta*, **60**, 1543-1552.

Ries, J.B. (2011) A physicochemical framework for interpreting the biological calcification response to CO_2-induced ocean acidification. *Geochim. Cosmochim. Acta* **75**, 4053–4064.

Rohl A.L., Wright K., and Gale J.D. (2003) Evidence from surface phonons for the (2x1) reconstruction of the (101–4) surface of calcite from computer simulation. *Am. Mineral. (Letters),* **88**, 921–925.

Rollion-Bard C. and Erez J. (2010) Intra-shell boron isotope ratios in the symbiont-bearing benthic foraminifera *Amphistegina lobifera*: Implications for $\delta^{11}B$ vital effects and paleo-pH reconstructions. *Geochim. Cosmochim. Acta*, **74**, 1530-1536.

Rollion-Bard C., Chaussidon M. and France-Lanord C. (2003) pH control on oxygen isotopic composition of symbiotic corals. *Earth Planet. Sci. Lett.,* **215**, 275–288.

Rollion-Bard C., Chaussidon M., and France-Lanord C. (2011) Biological control of internal pH in scleractinian corals: Implications on paleo-pH and paleo-temperature reconstructions. *C. R. Geoscience*, **343**, 397–405.

Sanyal A., Hemming N. G., Broecker W. S., Lea D. W., Spero H. J. and Hanson G. N. (1996) Oceanic pH control on the boron isotopic composition of foraminifera: Evidence from culture experiments. *Paleoceanography* **11**, 513-517.

Sanyal A., Hemming N. G., Broecker W. S. and Hanson G. N. (1997) Changes in pH in the eastern equatorial Pacific across stage 5-6 boundary based on boron isotopes in foraminifera. *Global Biogeochem. Cycles* **11**, 125-133.

Sanyal A., Bijma J., Spero H. and Lea D. W. (2001) Empirical relationship between pH and the boron isotopic composition of Globigerinoides sacculifer: Implications for the boron isotope paleo-pH proxy. *Paleoceanography* **16**, 515-519.

Saulnier S., Rollion-Bard C., Vigier N. and Chaussidon M. (2012) Mg isotope fractionation during calcite precipitation: an experimental study. *Geochim. Cosmochim. Acta*, **91**, 75-91.

Smith V. G., Tiller W. A. and Rutter J. W. (1955) A mathematical analysis of solute redistribution during solidification. *Can. J. Phys.* **33**, 723–745.

Spivack A. J., Palmer M. R. and Edmond J. M. (1983) The sedimentary cycle of the boron isotopes. *Geochim. Cosmochim. Acta* **51**, 1939-1949.

Stipp, S.L., Hochella Jr., M.F., Parks, G.A., and Leckie, J.O. (1992) Cd^{2+} uptake by calcite, solid-state diffusion, and the formation of solid-solution: Interface process observed with near-surface sensitive techniques (XPS, LEED, and AES). *Geochim. Cosmochim. Acta*, **56**, 1941-1954.

Stoll H.M., Rosenthal Y., and Falkowski P. (2002) Climate proxies from Sr/Ca of coccolith calcite: Calibrations from continuous culture of *Emiliania huxleyi. Geochim. Cosmochim. Acta*, **66**, 927–936.

Tang J., Köhler S.J., and Dietzel M. (2008a) Sr^{2+}/Ca^{2+} and $^{44}Ca/^{40}Ca$ fractionation during inorganic calcite formation: I. Sr incorporation. *Geochim. Cosmochim. Acta*, **72**, 3718-3732.

Tang J., Dietzel M., Bohm F., Kohler S.J., and Eisenhauer A. (2008b) Sr^{2+}/Ca^{2+} and $^{44}Ca/^{40}Ca$ fractionation during inorganic calcite formation: II. Ca isotopes. *Geochim. Cosmochim. Acta,* **72**, 3733-3745.

Tesoriero A.J. and Pankow J.F. (1996) Solid solution partition of Sr^{2+}, Ba^{2+}, and Cd^{2+} to calcite. *Geochim. Cosmochim. Acta*, **60**, 1053-1063.

Tripati, A., Eagle, R., Roberts, C., Li, G. (2011), A 20 million year long record of foraminiferal B/Ca ratios: Systematics and uncertainties in pCO_2 reconstructions, *Geochim. Cosmochim. Acta*, **75**, 2582-2610.

Tripati A., Roberts C., and Eagle R. (2009), Coupling of CO_2 and ice sheet stability over major climate transitions of the last 20 million years, *Science*, **326**, 1394-1397.

Watson E.B. and Liang Y. (1995) A simple model for sector zoning in slowly growing crystals: Implications for growth rate and lattice diffusion, with emphasis on accessory minerals in crustal rocks. *Am. Mineral.*, **80**, 1179-1187.

Watson E.B. (1996) Surface enrichment and trace-element uptake during crystal growth. *Geochim. Cosmochim. Acta*, **60**, 5013-5020.

Watson E.B. (2004) A conceptual model for near-surface kinetic controls on the trace-element and stable isotope composition of abiogenic calcite crystals. *Geochim. Cosmochim. Acta*, **68**, 1473-1488.

Watson E.B. and Müller T. (2009) Non-equilibrium isotopic and elemental fractionation during diffusion-controlled crystal growth under static and dynamic conditions. *Chem. Geol.*, **267**, 111–124.

Yu J. and Elderfield H. (2007) Benthic foraminiferal B/Ca ratios reflect deep water carbonate saturation state. Earth Planet. Sci. Lett. **258**, 73-86.

Yu J., Elderfield H. and Hönisch B. (2007a) B/Ca in planktonic foraminifera as a proxy for surface seawater. *Paleoceanography* **22**, doi:10.1029/2006PA001347.

Yu J., Foster G. L., Elderfield H., Broecker W. S. and Clark E. (2007b) An evaluation of benthic foraminiferal B/Ca and $\delta^{11}B$ for deep ocean carbonate ion and pH reconstructions. *Earth Planet. Sci. Lett*. **293**, 114-120.

Zeebe R., Wolf-Gladrow D. A., Bijma J. and Hoenisch B. (2003) Vital effects in planktonic foraminifera do not compromise the use of $\delta^{11}B$ as paleo-pH indicator: Evidence from modeling. *Paleoceanography* **18**, doi:10.1029/2003PA000881.

Zhong S. and Mucci A. (1989) Calcite and aragonite precipitation from seawater of various salinities: precipitation rates and overgrowth compositions. *Chem. Geol*., **78**, 283–299.

Figure Captions

Figure 1. Optical microscopy images of a calcite crystal from this study. A) Image collected after SIMS analyses to determine REE/Ca ratios. Black spots are the burn-marks from the six analytical profiles. Contours show the location of REE-spiked zones; B) Image collected after SIMS analyses to determine $\delta^{11}B$ ratios (profiles 1 and 2). Arrows correspond to the sequence of measurements (i.e., to the right and up). Appearance of REE element labels (Sm, La, Nd, and Tb) indicates mineral growth after the addition of the particular REE spike to fluid. The central zone of the crystal with outside Sm labels represents growth before addition of REE. The growth rate was determined by dividing the distance between two REE-spike in the calcite by the time elapsed between the two injections, e.g. $V_{Nd\text{-}Tb}=X_{Nb\text{-}Tb}/t_{Nd\text{-}Tb}$, where $X_{Nb\text{-}Tb}$ is the width of precipitated calcite between the injection of Nd and Tb, and $t_{Nd\text{-}Tb}$ is the time between these two injections. No data were collected on spot #13 in profile-2 (marked as X).

Figure 2. Fluid and SIMS data. Ca (a) and B/Ca (b) evolution in the fluid during experiment; t is the duration of the experiment assuming that t=0 at the addition of Sm spike. B concentration (in ppm) in the single calcite crystal (c). SIMS profile was performed between two opposite crystal edges (profile-3). No REE indicates the zone of crystal growth before any injection of REE-Spike into the solution. The labels 'Sm, La, Nd, Tb' stand for the time at which these REE-spikes were injected into the solution.

Figure 3. Dependence of boron partition coefficient ($D_B=B_{calcite}/B_{fluid}$) on crystal growth rate: A) B and Ca were measured together; B) ^{11}B data were corrected relative to (A) (see text for more details, section 2.3.3).

Figure 4. Growth Entrapment Model (GEM) simulation of our experimental data. D_B^{eq} and F are the equilibrium D_B and surface enrichment factor, respectively calculated form the data of Hemming et al. (1998). D_s is the diffusion of B in the calcite near surface layer. All experimental data are combined on this plot.

Figure 5. GEM simulation of the experimental data from Hemming et al. (1998). D_B(a′-b′/a-b) is the ratio of apparent partition coefficients between a′-b′ and a-b non-equivalent vicinals of $\{10\bar{1}4\}$ calcite face. Growth rates of faces a′-b′ and a-b are $V_{a'\text{-}b'}$ and $V_{a\text{-}b}$ respectively.
$V_{a\text{-}b} = 15 \cdot V_{a'\text{-}b'}$ (according to geometry model from Reeder (1996), i.e. 0.1 on X-axis below corresponds to $V_{a'\text{-}b'}$=0.1 nm/s and $V_{a\text{-}b}$=1.5 nm/s

Table 1. Composition of the fluid used for calcite precipitation experiments.

sub-sample	t days	Ca ppm	pH (NBS)	DIC µmol/kg	CO_3^{2-} µmol/kg	Ω	B, ppm	B/Ca mol/mol
Initial	-43	327.3	5.5	168	0.01	$1.4 \cdot 10^{-4}$	56.4	0.639
Sm-spike	0	244.0	8.00	n/a	n/a	n/a	43.1	0.633
La-spike	24	n/a	8.02	n/a	n/a	n/a	42.5	n/a
Nd-spike	35.8	157.5	8.06	2410	170.2	1.95	40.5	0.981
Tb-spike	85.9	143.9	8.15	2685	229.9	2.40	42.1	1.074
Final	149.9	95.2	8.17	2775	247.8	1.71	40.2	1.623

t is the time of crystallization from the addition of Sm spike. Ω is the fluid saturation state with respect to calcite.
Initial time was estimated as 43 days prior Sm addition by visual monitoring of the experimental flask with naked eye every 1-8 days. The onset of calcite precipitation was assumed to occur at -8<t<0 days.
Sm, La, Nd, and Tb correspond to the fluid sub-sample collected just before addition of REE.
DIC is dissolved inorganic carbon concentrations.
CO_3^{2-} and Ω calculations were performed using an excel implementation of CO2SYS (Lewis and Wallace 1998), modified to use measured calcium concentrations. The constants of Millero (1995) were used for the carbonate and sulfate system, respectively. Salinity (S) of 29.4 ‰ was estimated from the amount of salts added into the initial fluid. The solubility product of calcite (K_{sp}^*) was calculated using the expression developed by Mucci (1983), yielding pK_{sp}^* of 6.46. The pK_{sp}^* and Ω values presented here are more relevant to studied system than those presented in Gabitov et al. (2012).
Initial fluid was not exposed to a CO_2-containing atmosphere. pH of the fluid at the onset of crystallization was estimated to be 7.96±0.06, which is the average of pH values at t=-8 and t=0 days.
ICP-OES instrumental 1σ=0.2 %, dilution error is 5%.

Table 2. B concentration and isotopic composition within a single REE-spiked calcite crystal. SIMS profiles were measured between the edges of the crystals.

L (μm)	D_B	s.e.	$\delta^{11}B$ (‰)	2s.d.	L (μm)	D_B	s.e.	$\delta^{11}B$ (‰)	2s.d.	L (μm)	D_B	s.e.
		Profile-1*					Profile-2*				Profile-3	
40	0.366	0.073	-10.86	2.62	40	0.462	0.092	-10.37	1.66	30	0.263	0.038
130	0.516	0.103	-8.99	2.82	134	0.738	0.148	-9.99	1.46	80	0.394	0.056
194	0.638	0.128	-9.19	2.88	212	0.809	0.162	-7.69	1.16	135	0.578	0.083
228	0.669	0.134	-8.69	2.64	269	0.739	0.148	-7.90	1.52	190	0.695	0.100
285	0.797	0.159	-9.55	2.76	346	0.654	0.131	-8.65	1.34	250	0.829	0.119
331	0.781	0.156	-9.93	2.66	417	0.695	0.139	-7.46	1.3	310	0.774	0.111
381	0.829	0.166	-9.56	2.76	496	0.652	0.130	-11.07	1.38	370	0.878	0.126
431	0.820	0.164	-10.32	2.62	585	0.722	0.144	-10.15	1.16	430	0.945	0.136
492	0.790	0.158	-9.84	2.68	808	0.274	0.055	-9.41	1.7	490	0.834	0.120
569	0.797	0.159	-10.55	2.5	922	0.723	0.145	-10.00	1.58	550	0.533	0.076
661	0.669	0.134	-9.46	2.68	1032	0.779	0.156	-9.74	1.2	610	0.773	0.111
745	0.639	0.128	-9.96	2.68	1136	0.703	0.141	-9.83	1.26	670	0.578	0.083
812	0.307	0.061	-6.00	2.82	1271	0.397	0.079	-7.09	1.62	770	0.815	0.117
882	0.504	0.101	-6.46	2.64						890	0.759	0.109
936	0.906	0.181	-9.89	2.68						990	0.288	0.041
983	0.963	0.193	-9.32	2.62						1050	0.379	0.054
1050	0.976	0.195	-9.00	2.44						1110	0.923	0.132
1136	0.936	0.187	-11.84	2.54						1170	0.911	0.131
1233	0.888	0.178	-8.22	2.44						1230	0.867	0.124
1315	0.741	0.148	-10.73	2.58						1290	0.811	0.116
1381	0.418	0.084	-7.90	2.82						1350	0.72	0.103
1440	0.269	0.054	-8.54	3.28						1405	0.562	0.081
										1465	0.308	0.044

(*) D_B was calculated from ^{11}B data relative to B/Ca data from profile-3 of the same calcite crystal.
SIMS analyses were performed as profiles between the edges of the crystals. For example distance L of 25 and 1467 μm corresponds to the opposite edges of the crystal, i.e. start and end of analytical profile. S.e. of D_B is the standard error of the single spot analysis s.e.=s.d./$\sqrt{n}$, where s.d. is the standard deviation and n is the number of analytical cycles in each analysis. S.e. of V is the standard error calculated from the comparison of growth rates in the opposite sides of the crystal of particular REE-spiked zone.

Table 3. Mean partition coefficients of boron for calcite crystal and fluid as measured between each REE-spiked zone.

REE	V (nm/s)	s.d.	logR (μmol/m^2/h)	s.e.	D_B mean	s.e.	n	$K_{B/Ca}\cdot10^4$	s.e
				Profiles*-1 and 2					
Nd-Tb	0.041	n/a[#]	3.52	n/a[#]	0.511	0.050	10	1.92	0.212
La-Nd	0.11	0.0065	4.04	0.026	0.822	0.033	3	3.79	0.244
Sm-La	0.13	0.0096	4.01	0.103	0.870	0.036	5	4.61	0.300
La-Nd	0.089	0.0065	3.98	n/a[#]	0.756	0.053	2	3.48	0.299
Sm-La	0.086	0.0096	3.91	0.100	0.718	0.021	5	3.80	0.220
				Profile-3					
Nd-Tb	0.038	0.0055	3.64	0.053	0.503	0.069	7	1.77	0.286
La-Nd	0.11	0.0026	4.04	0.026	0.820	0.019	4	3.78	0.209
Sm-La	0.13	n/a[#]	3.92	0.21	0.898	0.019	5	4.76	0.259

V and R are the crystal extension (growth) and bulk precipitation rates, respectively.
(*) D_B was calculated from ^{11}B data relative to B/Ca data from profile-3 of the same calcite crystal.
REE labels denote the calcite zone grew between additions of the two REE spikes. For example a label of "Nd-Tb" means that values for growth rates and fractionation factors presented in the row were determined from the calcite grown between the addition of spikes containing Nd and Tb. Data from Nd-Tb zones from profiles 1 and 2 were combined because of similar V values. The V uncertainties from the identical REE-spiked zones located at opposite sides of the crystal were calculated as 1 s.d. between two values of V. (#) s.d. is n/a because of identical V or R evaluated at the different sides of the crystal.
The s.e. of D_B is calculated from multiple spot analyses s.e.=s.d./$\sqrt{n}$, where n is the number of SIMS spot analyses in a particular REE-spiked zone. Similarly to the growth rate error, the s.e. of R is the standard error calculated from the comparison of bulk precipitation rates in the opposite sides of the crystal of a particular REE-spiked zone.
$K_{B/Ca}$ is presented for the data from profile-3 because Ca was not measured during analyses of profiles-1 and 2. Growth rates are not exactly the same as reported in Gabitov et al. (2012) (that work was based on the same experiment) because B SIMS profiles from present work did not exactly mimic X,Y,Z position of SIMS profiles of $\delta^{18}O$ in Gabitov et al. (2012).

A

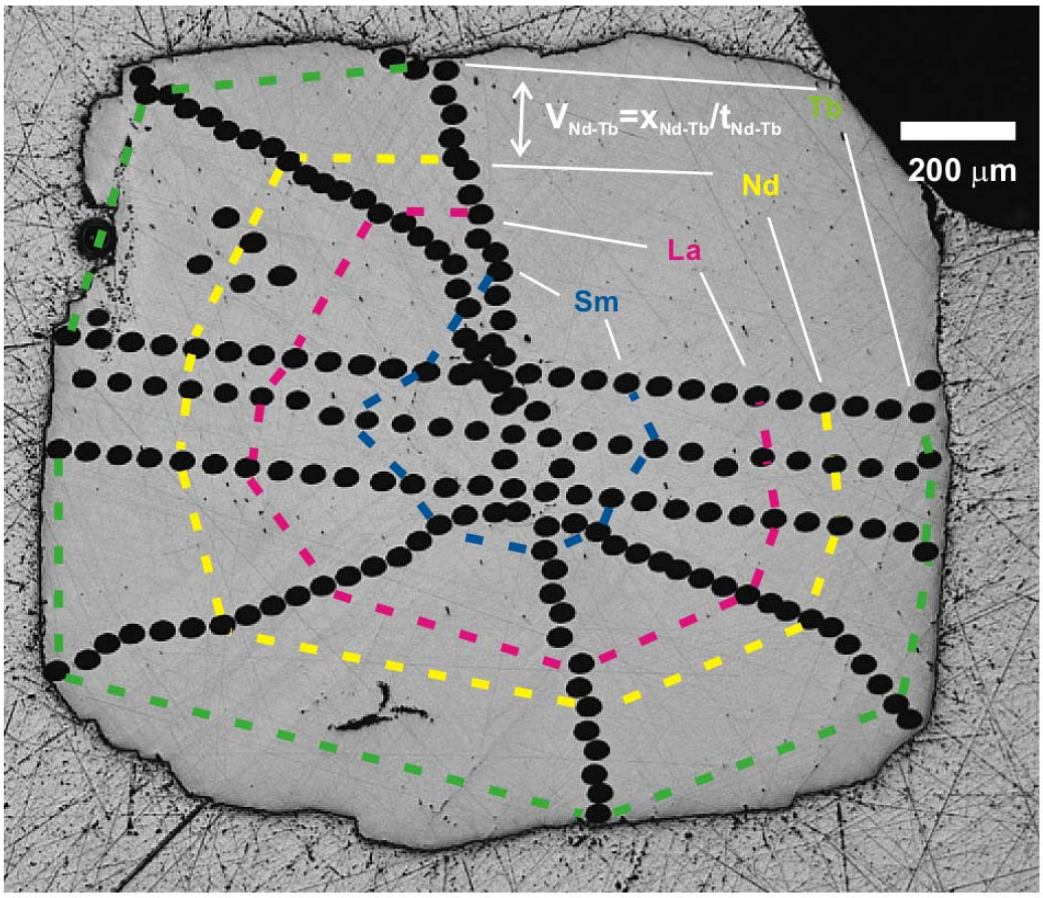
$V_{Nd-Tb}=x_{Nd-Tb}/t_{Nd-Tb}$
Tb
Nd
La
Sm
200 μm

B

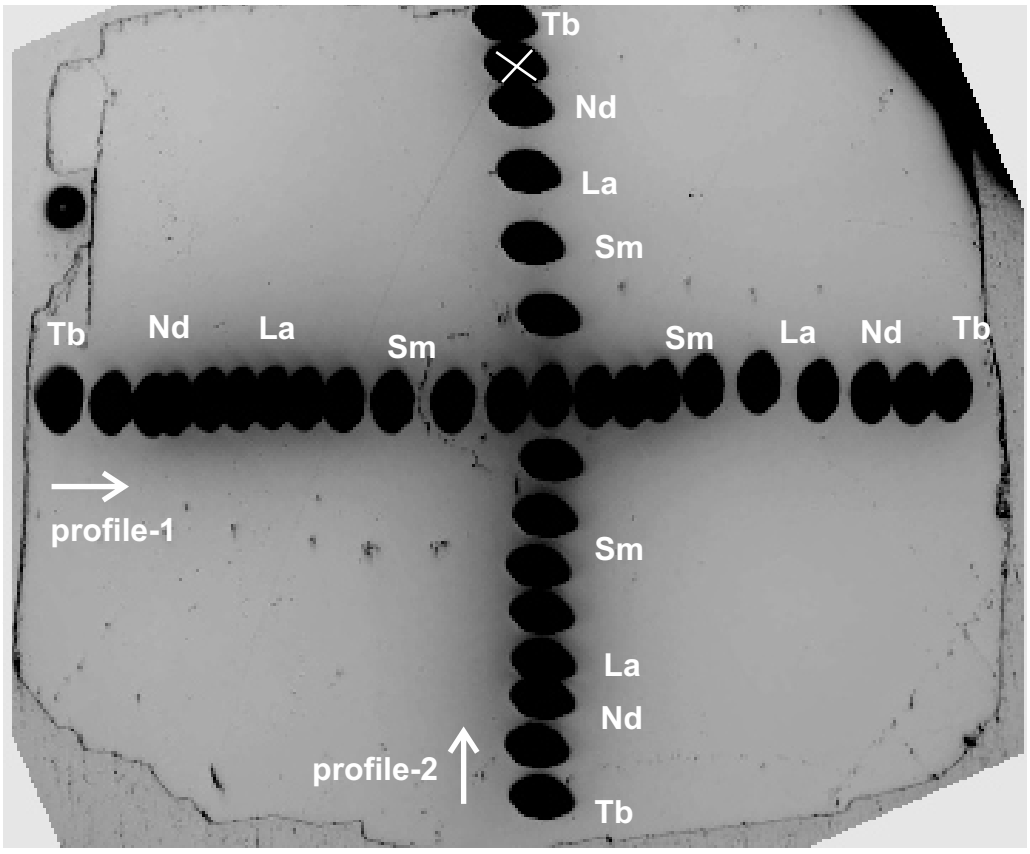
Tb
Nd
La
Sm
Tb
Nd
La
Sm
Sm
La
Nd
Tb
profile-1
Sm
La
Nd
profile-2
Tb

Figure 1

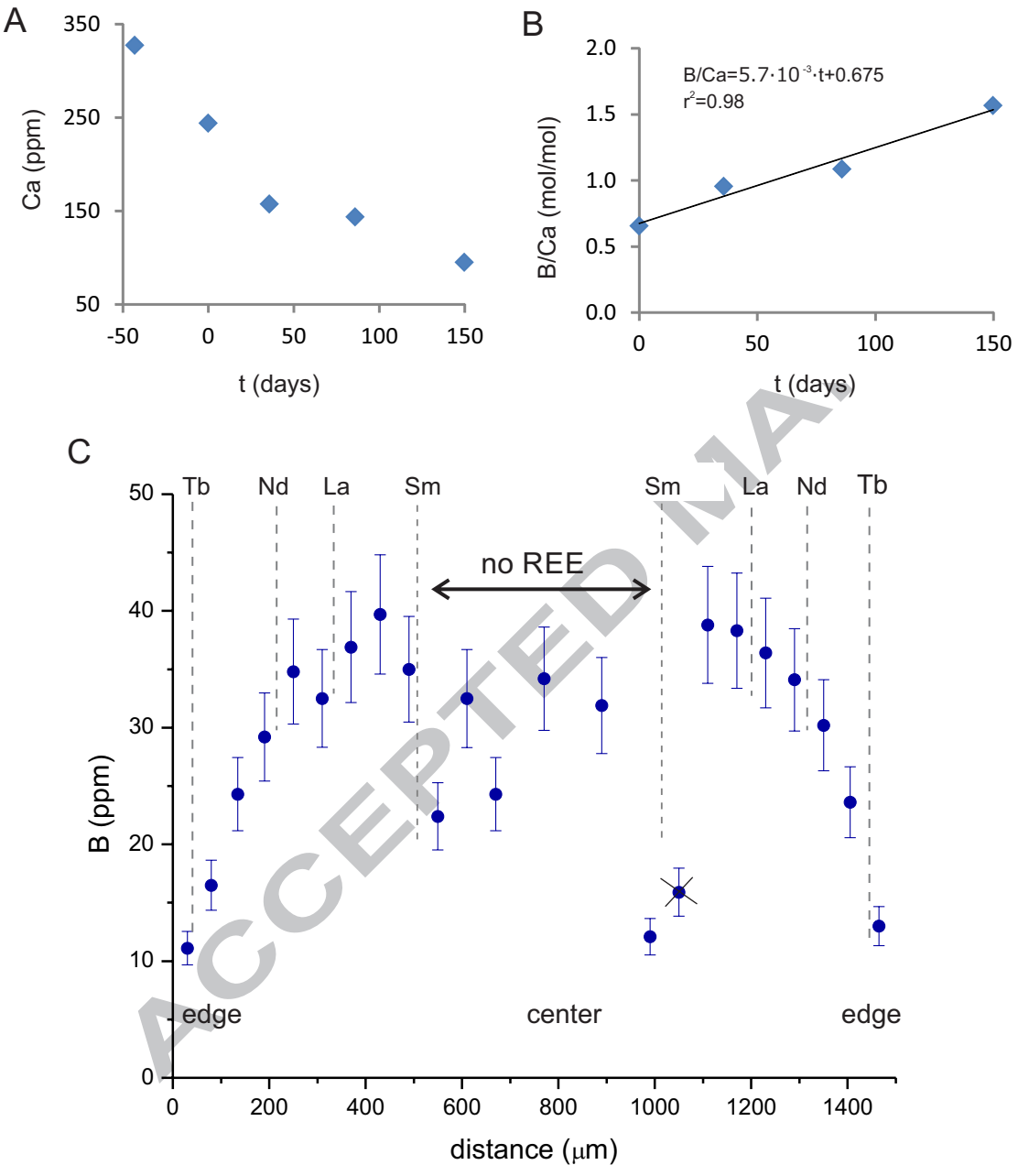

Figure 2

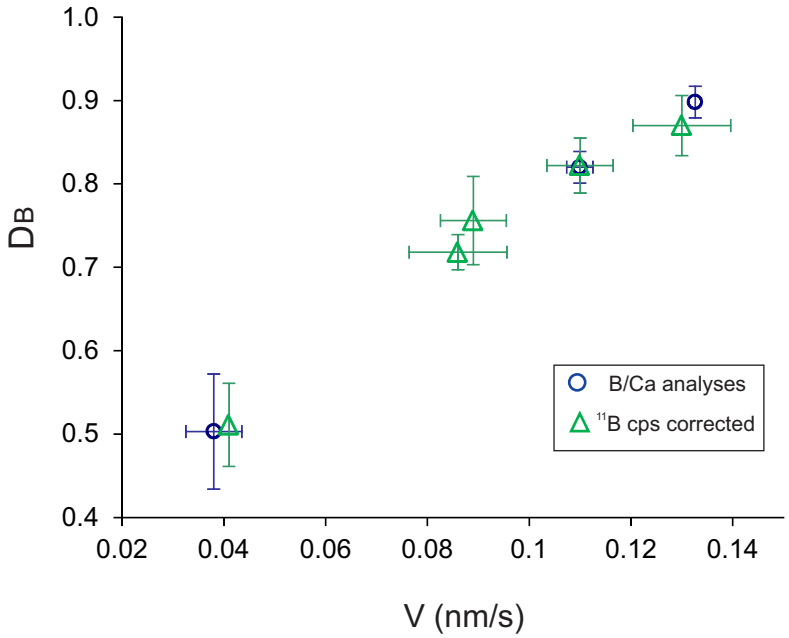

Figure 3

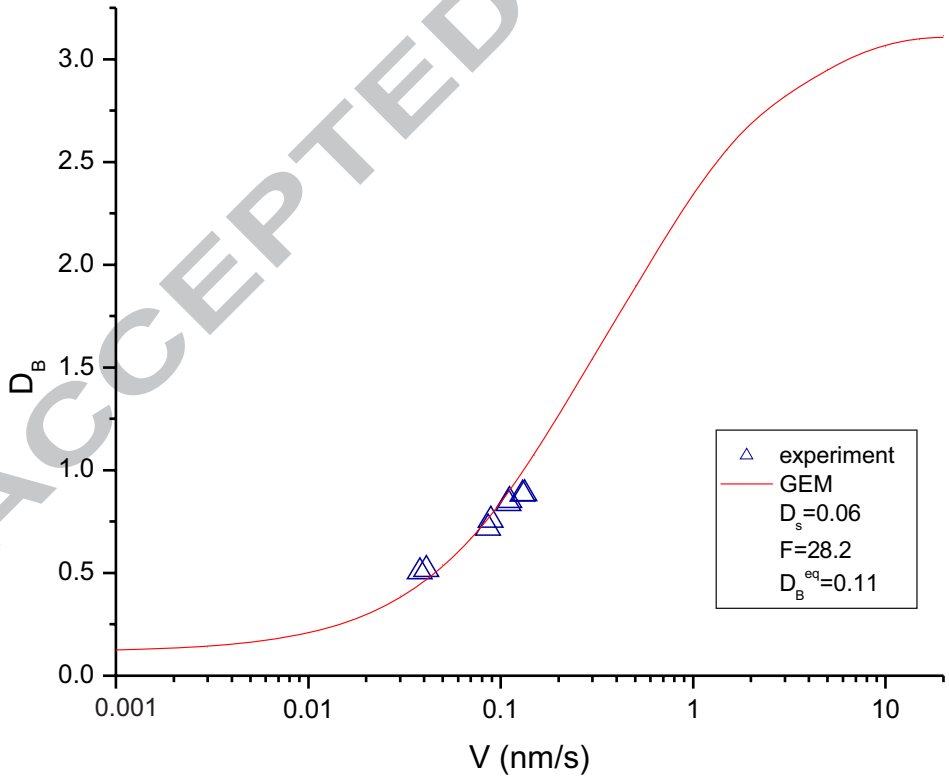

Figure 4

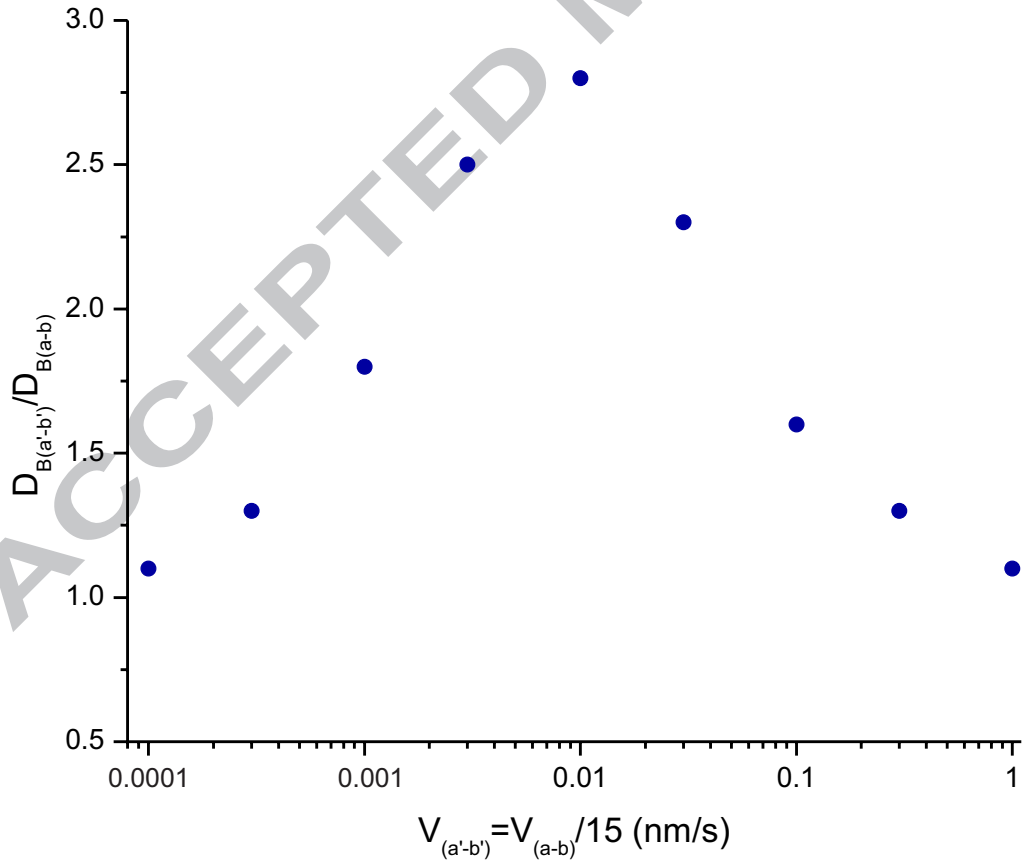

Figure 5